

Correlated Instanton Orientations in the $SU(2)$ Yang-Mills Vacuum and Pair Formation in the Deconfined Phase

Ernst-Michael Ilgenfritz¹, Stefan Thurner²

¹*Institute for Theoretical Physics, Kanazawa University, Japan*

²*Institut für Kernphysik, TU-Wien, Austria*

Abstract

Using the renormalization group motivated smoothing technique we study the semiclassical structure of the pure Yang-Mills vacuum. We carefully check that identified clusters of topological charge behave like instantons around their centers. Looking at distance distributions of clusters we find instanton-antiinstanton pair formation in the deconfined phase. We use suitably normalized gauge invariant field strength correlators to obtain first quantitative information on the relative color orientation of instantons. We give further evidence for a modified instanton profile in the confined phase and present a simple alternative model for it.

PACS number(s): 11.15.Kc, 12.38.Gc, 11.10.Wx, 11.10.Hi

Keywords: instanton liquid model, hadronic correlators, field strength correlators, vacuum structure, color orientation

The last decade has witnessed tremendous success in the practical application of the instanton model to describe hadronic physics [1–3]. This model is a radical simplification of QCD, taking just one specific feature of Yang-Mills theory into account, the existence of instantons [4]. Within this framework it is very natural to understand chiral symmetry breaking [5,6] (and its restoration at the hadronic phase transition) and to solve the $U_A(1)$ problem [7], but confinement has defied an explanation so far. The model has been formulated to represent a practical tool for a wide range of non-perturbative calculations at zero and non-zero temperature. Instanton models have been developed ranging from the random (uncorrelated) ideal instanton liquid model RILM [8], used mainly for zero temperature, to the interacting (correlated) instanton liquid model IILM [9], in particular for $T \neq 0$, when the temperature dependence of the interaction becomes important [10]. Even in the RILM there is some trace of interaction in so far as without some repulsive interaction [11] the existence of a distinguished instanton size could not be postulated.

Presently, some cornerstones of the IILM become subject of interest for lattice investigations and get immediate phenomenological importance. In deep inelastic scattering (DIS), attractive instanton-antiinstanton (valley) configurations within a narrow range of relative orientations, and the small size flank of the size distribution $d(\rho)$ are substantial for the event rate estimated for instanton mediated multiparticle processes [12]. Recently there was some effort to provide parts of this information, defining instanton size and distance distributions on the lattice, an enterprise which is under current debate [13–15].

The basic idea of instanton models is to reduce the infinite number of integration variables in the path integral, to an integral over a manageable set of relatively few collective coordinates. Those are attributed to instantons forming an interacting system that is described by the grand-canonical ensemble with the partition function

$$Z = \sum_{N_+, N_-} \frac{1}{N_+! N_-!} \prod_i^{N_+} \int [d\Omega_i^+ n(\rho_i^+)] \prod_j^{N_-} \int [d\Omega_j^- n(\rho_j^-)] \exp(-S_{\text{int}}). \quad (1)$$

Here $\Omega_i^\epsilon = (z_i^\epsilon, \rho_i^\epsilon, U_i^\epsilon)$ are the collective coordinates of the N_+ instantons ($\epsilon_i = +$) and N_- antiinstantons ($\epsilon_i = -$); z_i^ϵ are the center positions, ρ_i^ϵ the sizes and the $SU(N_c)$ matrices U_i^ϵ

the color orientations of (anti-)instantons. $n(\rho)$ is the semiclassical instanton distribution function [16]

$$dn_I = \frac{0.466 \exp(-1.679N_c)}{(N_c - 1)!(N_c - 2)!} \left(\frac{8\pi^2}{g^2}\right)^{2N_c} \exp\left(-\frac{8\pi^2}{g^2(\rho)}\right) \frac{d^4z d\rho}{\rho^5}. \quad (2)$$

The instanton interaction S_{int} can partly be taken into account in a cut-off single-instanton density function. The form

$$d(\rho) = \frac{1}{\rho^5} (\rho\Lambda)^b \exp\left[-\nu \frac{\rho^2}{\rho^2}\right], \quad (3)$$

results from a mean-field approximation [17] due to the instanton-instanton and instanton-antiinstanton interaction, being repulsive on average. b is the one-loop coefficient of the QCD β -function ($b = 11N_c/3$ for pure Yang-Mills theory), and $\nu = (b - 4)/2$. This results in a packing fraction $\frac{N}{V} \overline{\rho^2}^2 = \frac{\nu}{\beta} \frac{1}{\gamma^2}$, where the instanton interaction is measured by $\gamma^2 = \frac{27}{4} \frac{N_c}{N_c^2 - 1} \pi^2$ and $\beta = \beta(\bar{\rho}) \approx 15$ the average action per instanton. The color factor γ^2 represents the averaging over (relative) gauge orientations.

To compute mesonic correlation functions in this framework, Bethe-Salpeter equations [18] can be formulated in the so-called random phase approximation. For this purpose it is assumed that the instanton orientation is random and the distribution of instanton centers is uncorrelated. Baryonic correlation functions are difficult to obtain in this way. For crude estimates of the condensates, the knowledge of the instanton size distribution $d(\rho)$ (or simply the average ρ) and the distribution of distances (or the average nearest neighbor distance) is sufficient. Much of the knowledge about hadronic correlation functions [1] and about the spectral density [19] of the Dirac operator, however, has been obtained numerically, from Monte Carlo simulations of the instanton-antiinstanton liquid. Within this method of calculation it is possible to incorporate information on pair distributions in Euclidean and color orientation space which originates from specific Ansätze or is provided by lattice observations.

Very little was known, so far, about the relative color orientation. Concerning the quark mediated interactions, the fermionic determinant which enters a *non-quenched instanton*

Monte Carlo [6] can be reasonably parametrized in terms of the zero-mode overlap matrix element $T_{IA} \propto i(u_{\text{rel}}\Delta z)\rho^+\rho^-/(2\rho^+\rho^- + (\Delta z)^2)^2$ in order to sample instanton orientations *á la* Metropolis ¹. The gluonic part of the interaction is even less known, *i.e.* strongly dependent on the Ansatz of II or IA superposition. Usually it is taken care of by a sharp ρ -distribution (3) and by a hard-core cut-off [11]. The most important and remarkably Ansatz independent source of orientational interaction is the dipole-dipole interaction which acts exclusively between instanton and anti-instanton and does not contribute to the coefficient γ because the mean-field approximation neglects color correlations.

In this letter we give first quantitative results on the color correlation in instanton-instanton and instanton-antiinstanton pairs in pure Yang-Mills theory, which exists entirely due to gluonic interaction. Further we present the pair distribution between topological clusters as a function of distance in $4D$ space. Finally, we critically examine the assumed color coherence within a topological cluster. The progress in this paper towards a more detailed description of the instanton vacuum structure would not be possible without the method of constrained smoothing (CS) which makes use of the concept of perfect lattice action [20]. It allows to study semiclassical configurations which can be far from being exact solutions of the Euclidean field equations. Our Monte Carlo configurations are created with the same action using the Metropolis method. The CS procedure, in contrast to cooling or smearing, is essentially a two-lattice procedure, where lattice configurations are related to each other by blocking (fine-to-coarse) and inverse blocking [20] (coarse-to-fine). The smoothed configuration on the fine lattice, emerging from inverse blocking a blocked configuration, can be considered as *semiclassical*, which embraces deformations from classical solutions due to classical and quantum interactions. In the present work we want to get information about these interactions. In particular, nearby instanton-antiinstanton (AI) pairs will not be annihilated by CS. The distance and color correlations between these

¹ u_{rel} is the real 4-vector which represents the $SU(2)$ matrix U_{rel} and $\Delta z = z^+ - z^-$.

objects (as well as between instanton-instanton pairs) is not known from rigorous analytical calculations. Another possible deviation that we expect is a non-classical behavior of the field strength (lack of coherence) within a topological cluster which could give rise to a modified profile of an instanton. In contrast to CS, cooling does not converge before *locally classical fields* have been obtained. Therefore, a critical assessment of instantons in the quantum ensemble seems to be impossible. After some number of iterations, cooling or smearing destroy instanton-antiinstanton pairs. Therefore, based on these algorithms, it has been attempted to obtain detailed information on pair distance and ρ -distributions from a backward extrapolation of the cooling/smoothing history [14].

The second ingredient, which enables us to investigate the color correlation between clusters and to examine the coherence inside clusters, is borrowed from the stochastic vacuum approach [21]. In this approach, a gauge invariant field strength correlator (the non-local gluon condensate) has been proposed as a model independent characterization of the gauge theory vacuum. This correlation function has been studied on the lattice [22] using the cooling method. Presently we are calculating [23] the two-point correlator

$$D_{\mu\nu\rho\sigma} = \langle \text{Tr} (G_{\mu\nu}(x_1) S(x_1, x_2) G_{\rho\sigma}(x_2) S(x_2, x_1)) \rangle \quad (4)$$

where a Schwinger line phase factor $S(x_1, x_2) = P \exp \left[i \int_{x_2}^{x_1} dx_\mu A_\mu(x) \right]$ must be inserted. We use CS instead of cooling and the clover construction of the field strength components $G_{\mu\nu}^a$. In a semiclassical approximation [24], the leading contribution linear in $d(\rho)$ contains just all expressions as given by the classical instanton field, for instance - in the regular gauge - $G_{\mu\nu}$ replaced by

$$F_{\mu\nu}^{I,a} = -R^{ab} \eta_{\mu\nu}^b \frac{4 \rho^2}{(|x - z|^2 + \rho^2)^2}. \quad (5)$$

Here z and ρ have the meaning explained before, $\eta_{\mu\nu}^a$ is the 'tHooft symbol and $R^{ab} = \frac{1}{2} \text{Tr} (\tau^a U \tau^b U^+)$ is the adjoint representation of the global color orientation U of the instanton. To obtain the correlator (4), the instanton center z and radius ρ have to be averaged over with the density (3) after the phase factor $S(x_1, x_2)$ has been evaluated.

In the present work, once the centers of topological charge clusters are identified, the distribution of relative color orientations can be obtained by measuring (4) between the centers for pairs of clusters. The classical coherence of a cluster can be examined by measuring (4) between the center and some other point at a distance up to a few times ρ . While in the model the Schwinger lines for these cases are radial with respect to the instanton centers (and therefore $S(x_1, x_2) = 1$), the non-Abelian Schwinger phase cannot be neglected in the lattice configurations.

In all computations presented here we have used a simplified $SU(2)$ fixed point action on a $12^3 \times 4$ lattice [25], for which CS as described in [26] can be carried out in a theoretically consistent manner. Such actions provide scale invariant ideal instantons [20] and suppress dislocations [27]. Instantons with $\rho < 1.75 a$ (somewhat smaller than the blocked level lattice spacing) are unstable and cannot be made visible by CS. Our simulations were carried out in the confinement phase ($\beta = 1.4$ corresponding to a temperature $0.71 T_c$) and slightly above the critical temperature T_c ($\beta = 1.6, 1.15 T_c$). To identify instantons in smoothed but true quantum configurations we first looked for clusters of topological charge formed by lattice points with a charge density of equal sign above a certain threshold $q_{\text{thr}} = 0.015/a^4$ at $\beta = 1.4$ and $0.005/a^4$ at $\beta = 1.6$. Next, *connected* clusters are defined by a site-percolation routine. The search for local maxima $q_{\text{max}} = \max_x(q(x))$ inside the clusters identifies the instanton centers z_i . The instanton size can be obtained from q_{max}

$$\rho_i = \left(\frac{6}{\pi^2 |q(z_i)|} \right)^{\frac{1}{4}}, \quad (6)$$

as suggested by the classical profile. For all clusters we have measured a *cluster charge* $Q_{\text{cluster}} = \sum_{x \in \text{cluster}} q_L(x)$ and a *cluster volume* $V_{\text{cluster}} = \sum_{x \in \text{cluster}} 1$. Fig. 1 (top) shows the histogram of instanton radii according to (6). The left flank represents the probability to find high values of q_{max} . The cut-off at large ρ results from the chosen threshold value q_{thr} applied to the cluster search. The observed mean value in Fermi of $\bar{\rho}_{\beta=1.4} = 0.51$ fm is in good accordance with [13] where a similar ρ definitions was applied. It is larger than $\bar{\rho}$ reported in [14]. In deconfinement we find $\bar{\rho}_{\beta=1.6} = 0.40$ fm. Note that in the deconfinement

an $O(4)$ asymmetric profile becomes important, which might explain the unexpected shape of the ρ distribution ². Fig. 1 (bottom) shows how the observed clusters are clustering in the $V_{\text{cluster}}-Q_{\text{cluster}}$ plane. The solid line represents the relation between the two cluster properties predicted according to the classical instanton profile (5). The chosen threshold topological density has defined the horizontal scale, the total (unit) charge per cluster determines the vertical one. The dashed line is the result of a (somewhat deliberately chosen) Gaussian profile of a unit topological charge object. This curve makes clear why no cluster charge $Q_{\text{cluster}} > 0.4$ could be localized inside an individual cluster. The different performance of the two profiles gives an indication that in the quantum vacuum the instanton shape might be modified similarly to the freon model considered in Ref [17].

The coordinates of the cluster centers are used to measure histograms of relative distance for different pairings of cluster charges. The observed number of pairs per bin is compared to a random distance histogram. The random histogram was obtained by a simulation on 30000 configurations on the same lattice where the lattice coordinates of I (A) centers were chosen randomly all over the lattice with an appropriate density. The ratio is shown in Fig. 2 and represents the two-cluster distance distributions in both phases. (Here no distinction was made between time and spacelike separations). If there were no repulsion or attraction, $C(d)$ would be equal to unity. $C(d) > 1$ means attractive interaction (pair formation), $C(d) < 1$ repulsion. The situation for confinement is shown in the upper part. For II (AA) pairs no deviation from a random distribution is observed for $d > 3 a$. For the IA pairs there is a somewhat stronger repulsion up to $d = 3 a$ than for equal sign pairs. In the deconfinement (bottom) a peak is observed for the IA distance distribution, signaling the formation of IA pairs with a center-to-center distance of 2-3 lattice spacings (about 0.28 – 0.43 fm). For the same-sign case (II or AA) there is a slight repulsion at

²In present calculations we employ a characterization of cluster shape in the deconfinement that takes care of that.

short distances. This IA distance distribution might explain the drop of the topological susceptibility χ at the deconfinement phase transition as resulting from a local screening of topological charge. In our case $\chi_{\beta=1.4} = 1.0 \cdot 10^{-3}/a^4$ dropped to $\chi_{\beta=1.6} = 5.8 \cdot 10^{-5}/a^4$ over the transition.

We have modified the gauge invariant field strength correlator to a *normalized two-cluster overlap function* for any pair of clusters

$$\mathcal{O} = \frac{\langle \text{Tr} (G_{\mu\nu}(x_1) S(x_1, x_2) G_{\mu\nu}(x_2) S(x_2, x_1)) \rangle_{\text{pathes}}}{(\text{Tr} (G_{\rho\sigma}(x_1)^2))^{\frac{1}{2}} (\text{Tr} (G_{\tau\lambda}(x_2)^2))^{\frac{1}{2}}}, \quad (7)$$

were x_1 and x_2 denote the positions of the cluster-maxima. The Schwinger lines were chosen randomly among the shortest pathes connecting x_1 and x_2 and the average was done incoherently as indicated in (7). For a non-correlated ensemble of well-separated ideal instantons (II) or antiinstantons (AA) one would expect that \mathcal{O} averages to zero. In fact, due to the normalization (7) takes values in the interval $(-\frac{1}{3}, 1)$. This overlap is a measure for the normalized adjoint trace of the relative gauge orientation between the clusters, $\text{Tr}_{\text{adj}} U_{\text{rel}} = (\text{Tr} U_{\text{rel}})^2 - 1$. $\mathcal{O}_{II/AA} = -\frac{1}{3}$ corresponding to $\text{Tr} U_{\text{rel}} = 0$, and $\mathcal{O} = 1$ meaning $U_{\text{rel}} = \pm 1$ (color parallelity). Averaging with the normal Haar measure (no color correlation) would lead to $\langle \mathcal{O} \rangle = 0$. For an IA pair \mathcal{O}_{IA} is expected to be trivially zero, simply due to the opposite duality in $\eta_{\mu\nu}^a \bar{\eta}_{\mu\nu}^b = 0$, whatever the relative orientation is. In order to get access to the relative *color* orientation, in spite of this *color blindness* of (7), we perform a twist in the field strength of one of the clusters in the IA pair, changing $\vec{E}^a \rightarrow -\vec{E}^a$ before calculating the overlap (7).

In order to define U_{rel} , the relative orientation between the clusters, we introduce an $SU(2)$ matrix U into (7) and try to find, for each pair of clusters, the maximum of the function \mathcal{O}_U :

$$F = \max_U \mathcal{O}_U = \max_U \frac{\langle \text{Tr} (G_{\mu\nu}(x_1) U S(x_1, x_2) G_{\mu\nu}(x_2) S(x_2, x_1) U^+) \rangle_{\text{pathes}}}{(\text{Tr} (G_{\rho\sigma}(x_1)^2))^{\frac{1}{2}} (\text{Tr} (G_{\tau\lambda}(x_2)^2))^{\frac{1}{2}}}. \quad (8)$$

We find U as the rotational matrix needed to produce maximum overlap, *i.e.* to undo the relative color rotation U_{rel} . We found that \mathcal{O} *measured* for a cluster pair can be parametrized

as $\mathcal{O} = \frac{1}{3} (4 \cos^2(\alpha) - 1)$ in terms of $\cos(\alpha) = \frac{1}{2} \text{Tr } U$ as found by maximization with very good accuracy, for instance $\langle \mathcal{O} - \frac{1}{3} (4 \cos^2(\alpha) - 1) \rangle = -0.02 \pm 0.14$ for $\beta = 1.4$. In about 95% of all pairs of clusters, a rotation could be found turning F almost to unity. Only 5.4% of all clusters in the confinement phase were so incoherent that they reached values of $F < 0.8$. This is indirect support for the picture that the vast majority of the identified topological clusters contain all field strength components highly coherent in their center. We show in Fig. 3 the distributions in $\frac{1}{2} \text{Tr } U_{\text{rel}}$ for all pairs of clusters with a distance $d \leq 4 a$, found in the Monte Carlo sample in the confinement and in the deconfinement phase, compared with pairs with $d \leq 5 a$. The dashed line shows the distribution according to the normal Haar measure (no color correlation) which would lead to vanishing average of \mathcal{O} . The result is surprising in so far as in the confinement phase, opposite charge pairs are nearly uncorrelated while equal charge pairs correlated towards color (anti-)parallelity. The orientational alignment becomes stronger in the deconfined phase and is there roughly equal for both types of pairs. We are presently trying to identify the interaction parameters of S_{int} in (1) by instanton Monte Carlo simulations.

Finally we will examine the question to what extent the clusters themselves can be considered as classical, coherent fields also *outside* of their centers. It is assumed in the instanton model that, throughout the entire instanton, the color orientation of all field strength components follows the same U in (5). Corroborating what we have discussed in relation to Fig. 1 (bottom), we find here that the semiclassical picture has to be revised since the two-point field strength correlator inside a cluster has a profile which differs from the classical one. In order to define a correlation length within a topological cluster, we have modified the field strength correlator to a *normalized cluster profile*

$$\mathcal{P} = \frac{\text{Tr} (G_{\mu\nu}(x_1) S(x_1, x_2) G_{\mu\nu}(x_2) S(x_2, x_1))}{\text{Tr} (G_{\rho\sigma}(x_1)^2)} \quad (9)$$

pinning x_1 to the center of a cluster and considering it as a function of distance $d = |x_2 - x_1|$. For these calculations we restricted ourselves to on-axis displacements $x_2 - x_1$ such that no path averaging was necessary. No twist was applied to the field strength at x_2 such that

fields of opposite duality could not contribute. The resulting profile function is shown in Fig. 4 in the confinement (left) and deconfinement phase (right). Before final conclusions can be drawn the statistics of analyzed clusters has to be accumulated. The dashed line drawn in both figures represents a fit by a Gaussian profile function $\mathcal{P}(x) = \exp(-x^2/2\tilde{B})$. The squares show an average over the field strength profile of individual clusters described by $q_{\text{cluster}}(x) = \exp(-x^2/B)/(\pi^2 B^2)$, averaged over the empirical B distribution obtained from q_{max} . The solid line is the best fit to the average using the classical profile. This comparison substantiates our tentative model introduced to explain the $Q_{\text{cluster}}-V_{\text{cluster}}$ correlation in the confinement phase. Let us define a *r.m.s.* size (for weighting with respect to the topological density) of the instanton $\rho_{\text{rms}} = \sqrt{2\overline{B}}$. From the B distribution we obtain the average $\overline{B} = 2.71 a^2$ at $\beta = 1.4$. If the string tension is taken to be $\sqrt{\sigma} = 440$ MeV we find at $\beta = 1.4$ a lattice spacing $a = 0.23$ fm which corresponds to an $\rho_{\text{rms}} = 0.536$ fm. At $\beta = 1.6$ we find an average $\overline{B} = 2.87 a^2$. An extrapolation using the 2-loop formula gives $a = 0.142$ fm at $\beta = 1.6$ which results in $\rho_{\text{rms}} = 0.340$ fm. These numbers are very similar to the average radius defined via ρ according to (6) and its distribution, although the modification of the profile at large distances is of principal importance for the confinement phase. We have to stress the possibility of asymmetry effects changing the instantons in the deconfined phase. This was not yet taken into account in this feasibility study. We are currently studying shape and correlations by treating time and space directions separately.

In conclusion we emphasize that the use of constrained smoothing in combination with the measurement of gauge invariant two-point field strength correlators opens the possibility to obtain essential input information for semi-classically motivated models of QCD which was not available before.

We thank D. Diakonov and M. Müller-Preussker for initializing discussions and continued interest.

REFERENCES

- [1] E. V. Shuryak, Rev. Mod. Phys. **65**, 1 (1993); T. Schäfer and E. V. Shuryak, Phys. Rev. **D 54**, 1099 (1996).
- [2] D. I. Diakonov, Prog. Part. Nucl. Phys. **36**, 1 (1996), e-Print Archive: nucl-th/9603023.
- [3] T. Schäfer and E. V. Shuryak, Rev. Mod. Phys. **70**, 323 (1998).
- [4] A. A. Belavin, A. M. Polyakov, A. A. Schwartz, and Y. S. Tyupkin, Phys. Lett. **B 59**, 85 (1975).
- [5] C. G. Callan, R. Dashen, and D. J. Gross, Phys. Rev. **D 17**, 2717 (1978).
- [6] M. A. Nowak, J. J. M. Verbaarschot, I. Zahed, Nucl. Phys. **B 324**, 1 (1989); Nucl. Phys. **B 325**, 581 (1989); E. V. Shuryak and J. J. M. Verbaarschot, Nucl. Phys. **B 341**, 1 (1990); Nucl. Phys. **B 364**, 255 (1991).
- [7] G. 't Hooft, Phys. Rep. **142**, 357 (1986).
- [8] E. V. Shuryak and J. J. M. Verbaarschot, Nucl. Phys. **B 410**, 37, 55 (1993); T. Schäfer, E. V. Shuryak, and J. J. M. Verbaarschot, Nucl. Phys. **B 412**, 143 (1994).
- [9] E. V. Shuryak and J. J. M. Verbaarschot, Phys. Rev. **D 52**, 295 (1995); T. Schäfer and E. V. Shuryak, Phys. Rev. **D 53**, 6522 (1996); Phys. Rev. **D 54**, 1099 (1996).
- [10] E.-M. Ilgenfritz and E. V. Shuryak, Phys. Lett. **B 325**, 263 (1994); E. V. Shuryak and M. Velkovsky, Phys. Rev. **D 50**, 3323 (1994); T. Schäfer, E. V. Shuryak, and J. J. M. Verbaarschot, Phys. Rev. **D 51**, 1267 (1995); M. Velkovsky, E. V. Shuryak, Phys. Rev. **D 56**, 2766 (1997).
- [11] E.-M. Ilgenfritz and M. Müller-Preussker, Nucl. Phys. **B 184**, 443 (1981).
- [12] S. Moch, A. Ringwald, and F. Schrempp, Nucl. Phys. **B 507**, 134 (1997); A. Ringwald and F. Schrempp, presented at 6th International Workshop on Deep Inelastic Scattering and QCD (DIS 98), Brussels, Belgium, 4-8 Apr 1998, e-Print Archive: hep-ph/9805492.

- [13] P. de Forcrand, M. Garcia Perez, and I.-O. Stamatescu, Nucl. Phys. **B 499**, 409 (1997).
- [14] T. DeGrand, A. Hasenfratz, and T. G. Kovacs, Nucl. Phys. **B 505**, 417 (1997); Nucl. Phys. **B 520**, 301 (1998).
- [15] J. W. Negele, plenary talk given at 16th International Symposium on Lattice Field Theory (LATTICE 98), Boulder, CO, 13-18 Jul 1998.
- [16] G. 't Hooft, Phys. Rev. **D 14**, 3432 (1976).
- [17] D. I. Diakonov and V. Yu. Petrov, Nucl. Phys. **B 245**, 259 (1984).
- [18] D. I. Diakonov and V. Yu. Petrov, Nucl. Phys. **B 272**, 457 (1986); M. Hutter, Z. Phys. **C 74**, 131 (1997).
- [19] J. J. M. Verbaarschot, Acta Phys. Polon. **B 25**, 133 (1994); Nucl. Phys. **B 427**, 534 (1994).
- [20] T. DeGrand, A. Hasenfratz, P. Hasenfratz, and F. Niedermayer, Nucl. Phys. **B 454**, 587 (1995); Nucl. Phys. **B 454**, 615 (1995).
- [21] H. G. Dosch and Yu. A. Simonov, Phys. Lett. **B 205**, 339 (1988); Yu. A. Simonov, Nucl. Phys. **324**, 67 (1989); Yu. A. Simonov, Usp. Fiz. Nauk, **166**, 337 (1996); e-Print Archive: hep-ph/9709344.
- [22] L. Del Debbio, A. Di Giacomo, and Yu. A. Simonov, Phys. Lett. **B 332**, 111 (1994); A. Di Giacomo, E. Meggiolaro, and H. Panagopoulos, Nucl. Phys. Proc. Suppl. **54 A**, 343 (1997); Nucl. Phys. **B 483**, 371 (1997); M. D'Elia, A. Di Giacomo, and E. Meggiolaro, Phys. Lett. **B 408**, 315 (1997).
- [23] E.-M. Ilgenfritz and S. Thurner, to be published
- [24] E.-M. Ilgenfritz, B. V. Martemyanov, S. V. Molodtsov, M. Muller-Preussker, and Yu. A. Simonov, Phys. Rev. **D 58**, in print; e-Print Archive: hep-ph/9712523.

- [25] E.-M. Ilgenfritz, H. Markum, M. Müller-Preussker, and S. Thurner, Phys. Rev. **D 58** ,
in print; e-Print Archive: hep-lat/9801040.
- [26] M. Feurstein, E.-M. Ilgenfritz, M. Müller-Preussker, and S. Thurner, Nucl. Phys. **B**
511, 421 (1998).
- [27] T. A. DeGrand, A. Hasenfratz, and De-cai Zhu, Nucl. Phys. **B 475**, 321 (1996);
Nucl. Phys. **B 478**, 349 (1996).

FIGURES

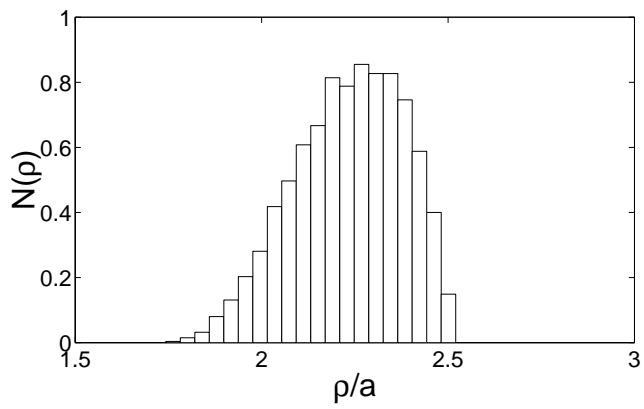
FIG. 1. Top: Instanton size distribution according to (6) in lattice spacings. The threshold values were $q_{\text{thr}} = 0.015$ in the confinement (left) and 0.005 in the deconfinement phase (right) such that instantons with radius $\rho > 2.523 a$ or $3.321 a$ are not visible. Bottom: average and variance of a scatterplot of Q_{cluster} vs. V_{cluster} . The agreement with the curve predicted by the classical profile (solid line) is lost for $V_{\text{cluster}} > 8$. A Gaussian instanton profile (dashed line) fits the data better in the confinement phase. Note that only 6.4% of the total number of clusters analyzed had a cluster volume $V_{\text{cluster}} > 8$.

FIG. 2. Distance distribution $C(d)$ for equal charge (II and AA) and opposite charge (AI) pairs in the confinement (top) and deconfinement phase (bottom). The peak in the deconfinement phase for AI pairs indicates pair formation. Results obtained from 8930 clusters (1000 independent configurations) at $\beta = 1.4$ and 8862 clusters (2000 configurations) at $\beta = 1.6$.

FIG. 3. Distribution in $\text{Tr } U_{\text{rel}}$ for II(AA) and AI pairs in the confinement (top) and deconfinement phase (bottom) averaged over all relative displacements $d \leq 4 a$ (fat line) and $d \leq 5 a$ (thin line). The random distribution (dashed line) is shown for comparison.

FIG. 4. Cluster profile \mathcal{P} (circles) obtained according to (9) from 100 independent configurations containing $O(1000)$ clusters at $\beta = 1.4$ (left) and containing $O(300)$ clusters at $\beta = 1.6$ (right). Solid lines are fits to the classical profile with free parameter ρ , dashed curves correspond to the best fit to a Gaussian profile with free parameter \tilde{B} . Squares represent the averages over Gaussian profiles according to a B distribution obtained from q_{max} for each individual cluster.

$\beta = 1.4$



$\beta = 1.6$

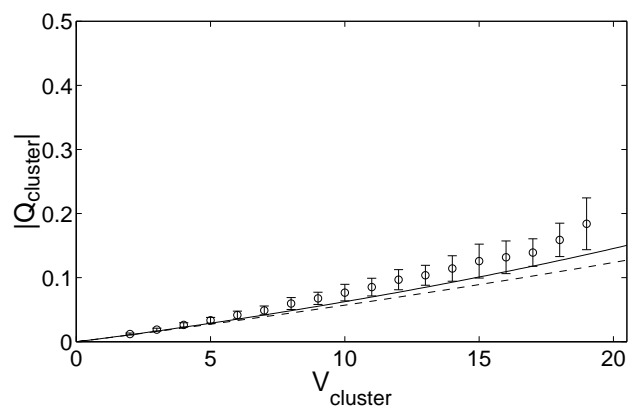
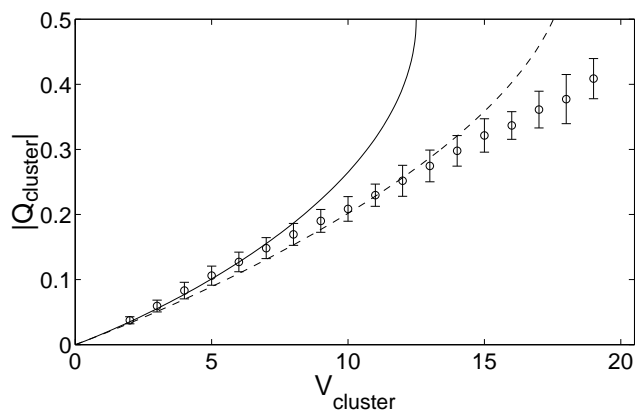
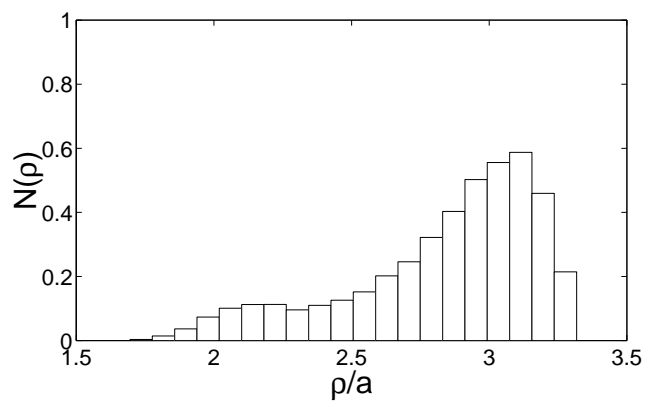


FIG. 1

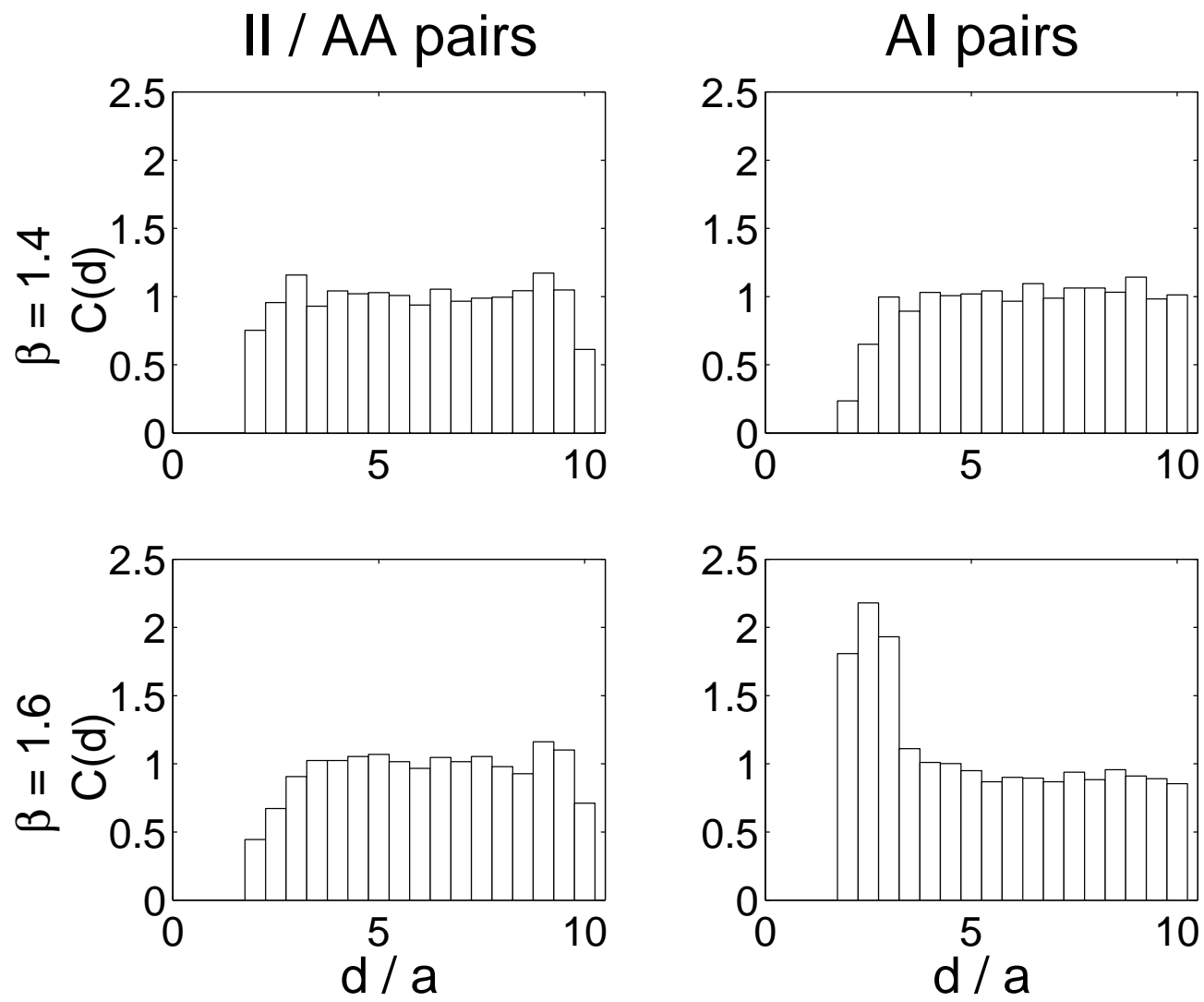


FIG. 2

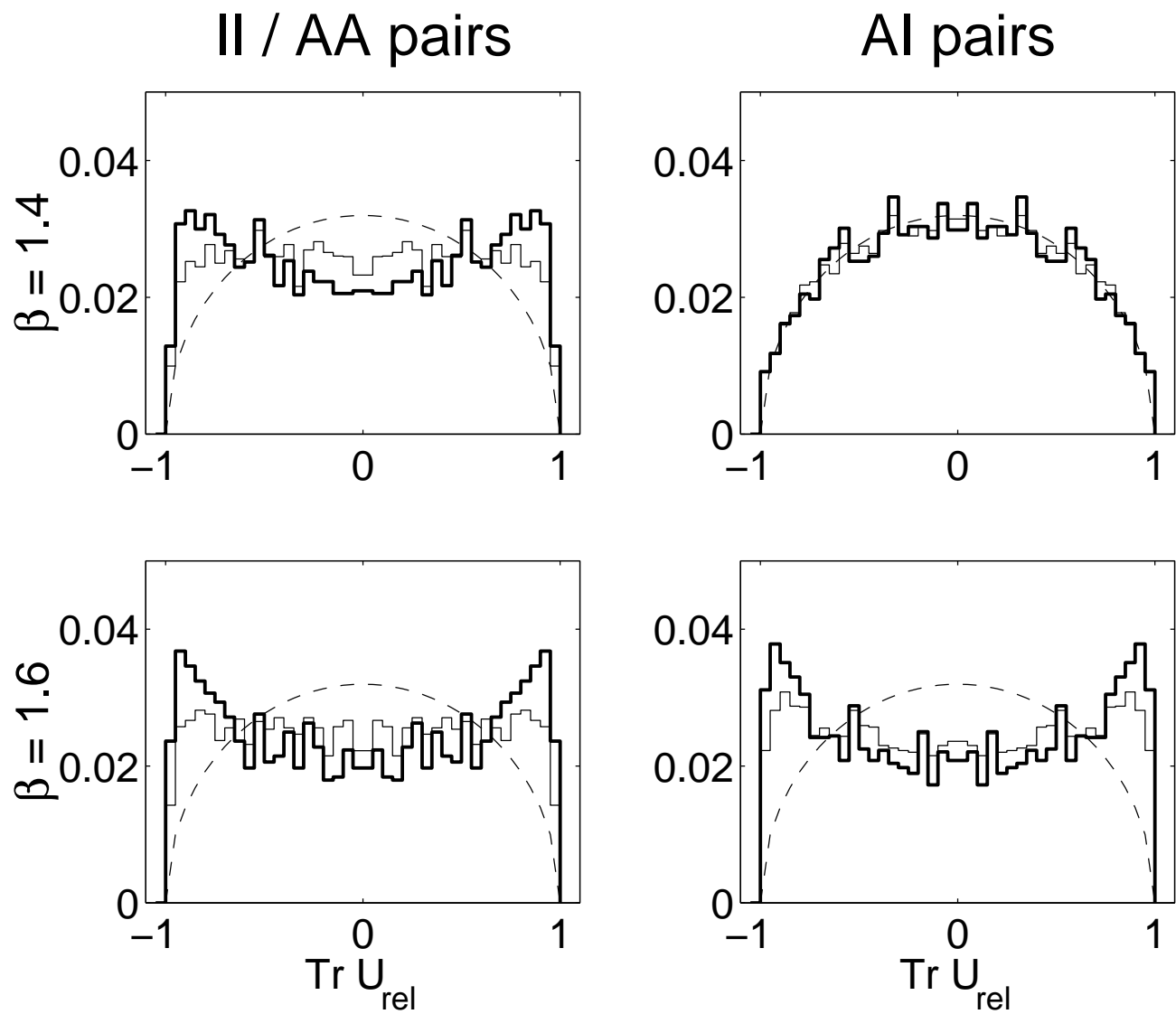
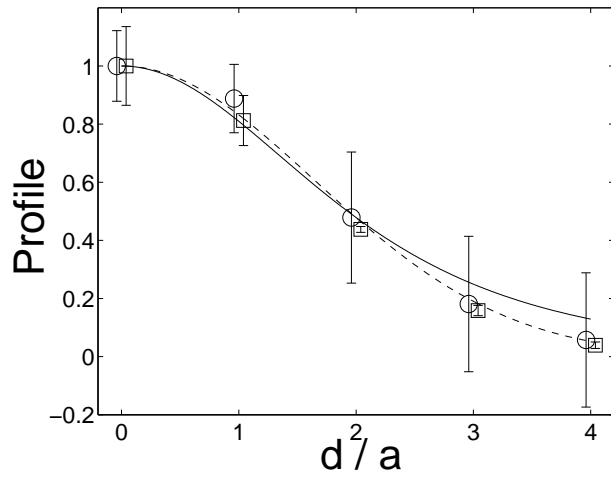


FIG. 3

$\beta = 1.4$



$\beta = 1.6$

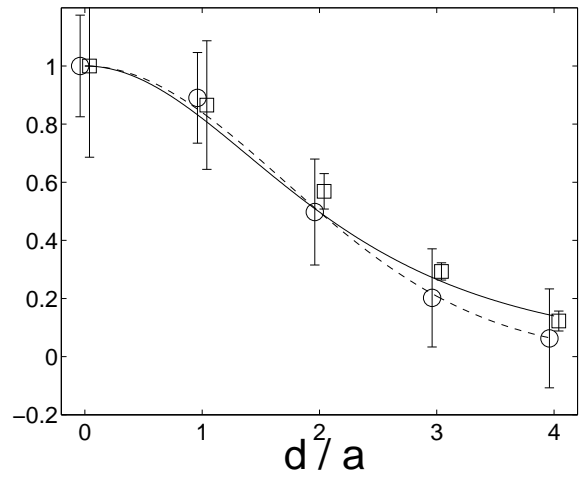


FIG. 4